JOURNAL OF CATALYSIS 80, 194–206 (1983)

The Textural Promotion of Metallic Iron by Alumina

W. S. BORGHARD AND M. BOUDART[1]

Department of Chemical Engineering, Stanford University, Stanford, California 94305

Received August 20, 1981; revised October 5, 1982

Textural promotion of iron catalysts, i.e., maintenance of high specific areas of reduced iron samples, is achieved by dissolved Al_2O_3 into Fe_3O_4 prior to reduction. A 10.2 wt% Al_2O_3 in Fe_3O_4 sample with a known surface composition in the reduced state was investigated to determine the mode of textural promotion of reduced iron by alumina. The amount of Fe^{2+} inside the reduced iron crystallites was determined to be approx 1 wt% by Mössbauer effect spectroscopy. X-Ray line broadening indicated a 61 ± 3-nm crystal size in agreement with the BET particle size of the same sample. The paracrystallinity following Hosemann was determined to be 0.6, a value in agreement with an empirical correlation between particle size and paracrystallinity. All data presented here are compatible with Hosemann's view that molecular inclusions of $FeAl_2O_4$ in the iron lattice are responsible for textural promotion. Since particle size is inversely proportional to specific surface area, paracrystallinity may be a dominant cause of textural promotion in our case. Another cause may be a patchy monolayer of alumina at the surface of the iron particles, preventing sintering by a "skin" effect.

INTRODUCTION

Ammonia synthesis catalysts are usually prepared by fusing magnetite, Fe_3O_4, with unreducible promoters followed by reduction of the magnetite to metallic iron. One of these promoters is alumina, Al_2O_3. Addition of 2–3 wt% Al_2O_3 to Fe_3O_4 increases the specific surface area of reduced iron by a factor of 5 (*1*). Since the activity of surface iron toward ammonia synthesis does not change with the addition of Al_2O_3 (*1, 2*), the latter is called a textural promoter, as it only improves the texture of the catalyst. However, the mechanism of textural promotion remains unclear. The first question is: where is the alumina after reduction of the sample?

To answer this question, several investigators have determined the surface composition of reduced samples. Emmett and Brunauer (*3*) have shown by selective chemisorption that iron occupies about 45% of the total surface area for a reduced sample containing originally 10.2 wt% Al_2O_3 in Fe_3O_4. This sample was designated No. 954. Solbakken *et al.* (*4*) determined the amount of surface oxygen by exchange between the latter and $H_2{}^{18}O$ for this same reduced sample. They confirmed the results of Emmett and Brunauer (*3*). Besides, by comparing successive exchanges with $H_2{}^{18}O$ on alumina and on a similar sample, they concluded that the Al_2O_3 at the surface of the promoted sample exists in a fractional monolayer or thin "skin." On the basis of that, a large amount of the total Al_2O_3 is located either in large crystals of Al_2O_3 or inside the iron crystals, since 60% of a monolayer of Al_2O_3 accounts for only 0.5% of the total 10.2%. Using Auger electron spectroscopy (AES) on sample No. 954, Silverman and Boudart (*5*) confirmed the earlier results of Emmett and coworkers. The surface composition of the reduced samples led to the "old" model of textural promotion (*1*) (Fig. 1a). Sintering is depressed because the alumina skin acts as a "spacer" between iron surfaces.

In 1966 Hosemann *et al.* (*6*) introduced a new concept: paracrystallinity. If a crystal lattice contains substitutional point defects, the interplanar spacings change and a strain field exists in the vicinity of the defect.

[1] To whom all correspondence should be addressed.

0021-9517/83/030194-13$03.00/0

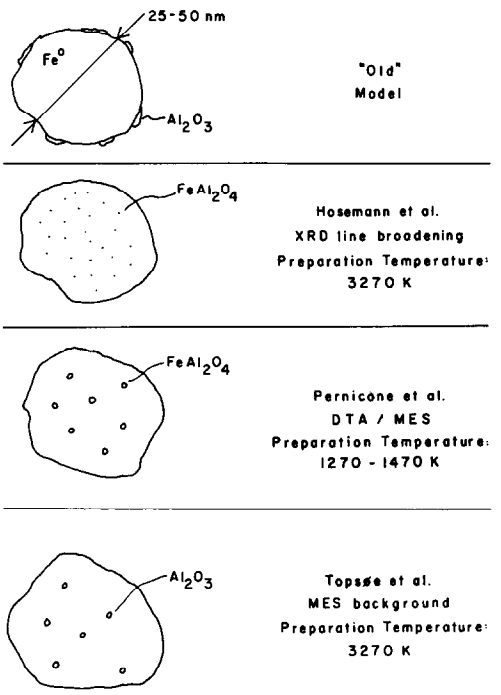

FIG. 1. Some models of iron–alumina materials.

Paracrystallinity is defined as the normalized standard deviation of a crystallographic interplanar distance, and it is measured by the width of X-ray diffraction (XRD) lines (*7*) (Fig. 2). In the case of alumina-promoted iron, the seven atoms of a hercynite molecule, $FeAl_2O_4$, replace seven iron atoms in the body-centered cubic (BCC) crystal lattice to produce paracrystallinity (Fig. 3). Since the volume of one hercynite molecule is the same as that of seven iron atoms, there is no change in the average interplanar spacings or the size of the unit cube, a_0. Paracrystallinity in the

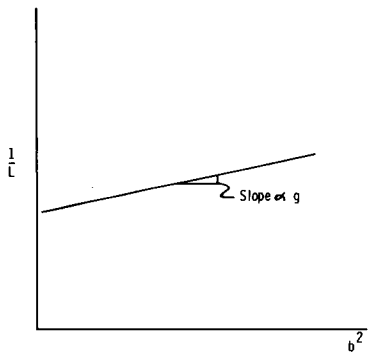

FIG. 2. Detection of paracrystallinity by X-ray diffraction. $b = 2\sin\theta/\lambda = n/d$; L = crystal size, g = paracrystallinity, λ = X-ray wavelength, 2θ = angle between X-ray source and sample, n = order of reflection, d = interplanar spacing.

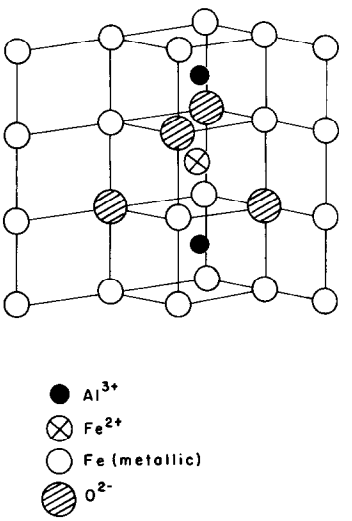

FIG. 3. Hercynite in the α-iron lattice.

110 direction of the α-iron lattice has been observed for a variety of iron–alumina materials (*6, 8–10*) including a commercial ammonia synthesis catalyst (*7*). Moreover, Buhl and Preisinger (*11*) examined a sample of Hosemann *et al.* (*6*) by secondary-iron mass spectroscopy (SIMS). Their data indicated that the aluminum and oxygen atoms existed as $FeAl_2O_4$ rather than Al_2O_3. Unfortunately, the state of reduction of the sample was unknown. These studies led to the suggestion that hercynite molecules inside iron crystals (Fig. 1b) are responsible for the textural promotion of iron (*9*), as indicated by a correlation between iron crystal size and paracrystallinity.

This correlation is shown in a plot of iron crystal size, L, vs paracrystallinity, g, (Fig. 4) which shows that L decreases linearly as g increases. The data are from Hosemann *et al.* (*6, 9*) and Pernicone *et al.* (*8, 10*). A similar correlation has been reported by Fischer *et al.* (*7*) who plotted the square root of N vs $1/g$, where N (= L/d) is the number of planes in the crystal with interplanar spacing d (202.66 pm for the 110 direction of α-Fe). They drew two straight lines through the origin to encompass their data obtained with catalysts, polymers and graphite. These lines have slopes, α^*, of 0.10 and 0.20. The relation between $\sqrt{N}$ and g, called the α^* law by Hosemann *et al.* (*12*), must be considered as an empirical finding. A theoretical attempt to relate crystal size with strain field of paracrystallinity was made by Schultz (*13*) who assumed that the point defects were hard spheres with radii slightly larger than the substituted group of atoms. He calculated the strain energy for one $FeAl_2O_4$ substitution or defect. The fraction of defects that produce strain was determined by assuming that if a defect was sufficiently close to the surface (1 to 4 defect radii), the strain was relaxed. For a single crystal, the strain energy was added to the iron interfacial energy, and this sum was minimized with respect to the crystal size. The result is a plot of equilibrium crystal size vs defect concentration. For a sample with 3 wt% Al_2O_3 in iron, the crystal size should be less than 10 nm. Although the predicted crystal size is lower than that measured by XRD (20–50 nm), Schultz suggested that the theory was qualitatively correct (*13*).

Hosemann's model of Al_2O_3-promoted iron has been modified by two groups of workers who examined similar samples by

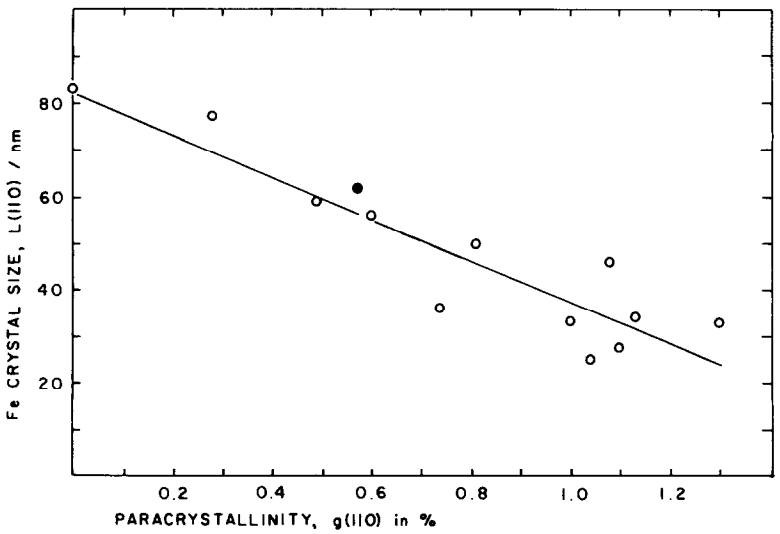

FIG. 4. Iron crystal size vs paracrystallinity. (O) Data taken from Hosemann *et al.* (*6, 9*) and Pernicone *et al.* (*8, 10*), (●) this study.

Mössbauer effect spectroscopy (MES). In both cases no collapse in the metallic iron magnetic field was detected. Such a collapse would be expected if enough $FeAl_2O_4$ molecules substituted for the magnetic iron. Pernicone *et al.* (*8, 10*) prepared their own iron–alumina samples by a precipitation technique followed by pretreatment in a CO/CO_2 mixture and reduction in H_2. They concluded that the alumina exists in iron as hercynite inclusions, ca. 25 nm in diameter, which would not affect the metallic iron magnetic field (Fig. 1c). Pernicone *et al.* (*8, 10*) also measured the temperature of the α/γ transition of metallic iron for their samples by differential thermal analysis (DTA). They found that this temperature was higher for the samples with Al_2O_3 than for those without. Also, successive DTA runs lowered the transition temperature of the promoted samples to the transition temperature for unpromoted samples. These results suggest that the Al_2O_3 is inside the iron crystals and prevents the α/γ transition from taking place until higher temperatures. Topsøe *et al.* (*14*) obtained from Hosemann a sample (with g equal to 1.04%) and detected with MES a paramagnetic component in the background of the spectra. As this component was removed by complete reduction, they concluded that the hercynite inclusions described by Pernicone *et al.* (*8, 10*) could be reduced to Al_2O_3 inclusions under the proper conditions (Fig. 1d). However, Ludwiczek *et al.* (*9*) do not believe that these inclusions of Al_2O_3 or $FeAl_2O_4$ can produce paracrystallinity.

In summary, different samples have been examined by several techniques. As a result, four models have been proposed which describe the dominant location of the alumina in or on iron (Fig. 1). Also, these models imply two different modes of textural promotion of reduced iron by alumina: one by way of the "skin" effect and the other by internal strain. The important experimental techniques appear to be BET adsorption, selective chemisorption, MES, and XRD. Selective chemisorption by CO is used to measure the fractional iron specific surface area. The BET specific surface area can be used to calculate the *particle* size which is not necessarily equal to the *crystal* size. MES can be used to determine the amount of iron that exists as Fe^{2+}. Results from XRD give the paracrystallinity and the iron crystal size. Thus far, four techniques have not been used on the same sample after complete reduction. The purpose of this work was to help decide between alternative models (Fig. 1) by means of MES and XRD of a well-reduced sample (954) which has already been studied by selective chemisorption (*3*) and related techniques (*4, 5*). The sample was obtained from J. Gryden at the Johns Hopkins University. It originally came from the Fixed Nitrogen Research Laboratory. It was prepared by fusing magnetite (Fe_3O_4) with 10.2 wt% alumina (Al_2O_3) at ca. 1820 K (*2*). This sample has been studied extensively (*2–5, 15–17*). In the reduced state, it has a specific surface area of 8.8 $m^2\ g^{-1}$ the weight being that of the unreduced sample (*4*). Approximately 45% of the surface consists of iron (*3–5*).

EXPERIMENTAL

Mössbauer Effect Spectroscopy

The iron–alumina sample was finely ground (0.05–0.10 mm) and mixed with Graphon (a graphitized carbon from Cabot Corp.). The Graphon acted as a diluent in order to produce an areal density of 14.3 mg of natural Fe per square centimeter. A sample, 0.2931 g, of the mixture was pressed into a 2.85-cm^2 wafer which was mounted in a flow through quartz cell. This cell allowed *in situ* control of temperature and gas composition. The sample was heated by an external electric heater that enclosed the cell. A temperature controller held the temperature at 698 K during the reductions. The temperature was measured by a Chromel–Alumel thermocouple positioned just above the wafer.

The sample was always examined at room temperature in helium except for the unreduced sample which was examined in air. The sample was examined in the unreduced state (as is) and after each of several reductions. The reductions were always done at 698 K, in flowing dihydrogen, at ambient atmospheric pressure, and at a volumetric space velocity of 100 s^{-1} in the following manner.

The sample was heated to 698 K in flowing helium. Then, the flowing gas was switched from He to H_2. After the desired amount of time had passed, the flowing gas was switched back to He, and the temperature controller was turned off, allowing the sample to cool in flowing helium. The H_2 (99.99% from Liquid Carbonic) was purified by passing it through a heated palladium membrane (Milton Roy hydrogen purifier). The helium (99.995% from Liquid Carbonic) was passed over freshly reduced copper turnings heated to 425 K to remove oxygen and then through a molecular sieve trap at 78 K to remove water.

The sample was reduced 11 times for the following amounts of cumulative time in hours: 0.25, 0.50, 1.50, 4.5, 7.5, 10.5, 13.5, 16.5, 19.5, 25.5, 31.5. After every reduction, two spectra were taken at room temperature between + and −10 and mm s^{-1} and between + and −3 mm s^{-1} except for the first reduction where only one spectrum was taken between + and −10 mm s^{-1}. The smaller range (between + and −3 mm s^{-1}) permitted higher resolution of that velocity range in which Fe^{2+} in FeO or $FeAl_2O_4$ would be detected either as distinct peaks or in the background.

A 25.4-μm-thick iron foil (99.9%) and pure Graphon were also examined by MES at room temperature in air.

The Mössbauer effect spectrometer used in this experiment has been described before (*18*). The essential details are given below. The source of ^{57}Co diffused into a rhodium foil obtained from New England Nuclear though Austin Science Associates (ASA). The gamma rays were directed through the sample and counted with a Kr–CO_2 filled proportional counter. The source was mounted on the drive shaft of an ASA Mössbauer spectrometer velocity transducer drive. It was run in constant acceleration mode resulting in two mirrored spectra for each MES run. The velocity was measured by a laser interferometer (ASA). The velocity counts from the laser system were stored in every sixteenth channel. The laser signal together with the gamma ray counts and counts from an oscillator were stored in a 512-channel multichannel analyzer (MCA) with a multiplexer. Time counts from the oscillator were stored in five channels.

The data collected in the MCA were transferred to a PDP 11/34 minicomputer where they were analyzed. A computer program fitted the data to Lorentzian lines plus a parabolic background.

The MES peaks were labeled numerically from negative velocity to positive velocity, the latter defined as motion of the source toward the absorber. For hyperfine spectra the magnetic field (H), the isomer shift (δ), and the quadrupole interaction (ε) are defined as

$$H = (v_6 - v_1) \times 3.109 \text{ T}$$

$$\delta = (v_1 + v_2 + v_5 + v_6)/4 \text{ mm s}^{-1},$$

$$\varepsilon = (v_1 - v_2 - v_5 + v_6)/4 \text{ mm s}^{-1},$$

$$A_T = \pi/2 \sum_i (\text{Dip}_i \times \text{Width}_i) \text{ mm s}^{-1},$$

where v_i is the position of the ith peak in millimeters per second with respect to the source, and A_T is the total area of the magnetic component. For quadrupole doublets the isomer shift (δ) and the quadrupole splitting (QS) are defined as

$$\delta = (v_1 + v_2)/2 \text{ mm s}^{-1},$$

$$\text{QS} = (v_2 - v_1) \text{ mm s}^{-1}.$$

X-Ray Diffraction

The XRD experiments were performed with a Picker X-ray diffractometer using

Cu$K\alpha$ radiation. This diffractometer was automated with a PDP 11/03 minicomputer and Canberra interface equipment. The metallic iron 110 and 220 reflections were measured by counting at 0.025° (2θ) intervals. For the Fe 110 reflection the range scanned in 2θ degrees was 43–46.5°. The same range for the 220 reflection was 97.5–100.5°. This resulted in 140 and 120 points, respectively. The diffracted X rays were counted for 10 s per point for the 220 reflection. At the 110 reflection counting was done for 2 and 4 s for an iron standard and the iron–alumina sample, respectively. These data were transferred to a PDP 11/34 minicomputer. There they were fitted to Gaussian, Lorentzian, and Lorentzian-square functions by a Marquardt optimization program in order to determine the linewidths more exactly.

Two peaks were resolved and corresponded to the Cu$K\alpha_1$ and Cu$K\alpha_2$ wavelengths. These data were best fitted by Lorentzian waveforms. The widths of the two peaks, $K\alpha_1$ and $K\alpha_2$, were constrained to be the same. The height of the first peak was also constrained to be twice the height of the second. These constraints forced the area of the first peak to be twice the area of the second as would be expected for $K\alpha_1$ and $K\alpha_2$ radiation. The linewidths of the 110 and 220 reflections were used to determine the crystal size, L, and the paracrystallinity, g, in the 110 direction according to the method of Fischer *et al.* (7). Explicitly, the linewidths were plotted against b^2 as in Fig. 2. The intercept was $1/L$, and the slope was $g^2\pi^2 a_0/\sqrt{2}$. Since the 330 reflection coincides with the 411 reflection, the 330 reflection could not be used. None of the higher reflections can be detected with Cu radiation.

A 5.37-g cylindrical slug of iron (99.9% from Alfa-Ventron Corp.) was rolled into a roughly rectangular shape: 15 mm × 38 mm × 1 mm thick. Then it was annealed at 1070 K in flowing helium (99.99% from Liquid Carbonic). This sample was used to determine the instrumental linewidth broadening. This linewidth was used to correct the linewidth measured for the reduced iron–alumina material. A small amount of the iron–alumina 3.486 g, was ground finely, placed in a Pyrex cell and reduced for 24 h in flowing dihydrogen a 698 K, atmospheric pressure, and a volumetric space velocity of 2.0 s^{-1}. The dihydrogen was palladium diffused in a Matheson hydrogen generator. After reduction, the sample was passivated in a 1% O_2/He mixture. The reduced, passivated sample was placed in a Plexiglas sample holder which has a 1-mm-deep rectangular well. The sample was held in place with Mylar film.

In order to determine the amount of oxygen taken up during passivation, this sample was analyzed by thermal gravimetric analysis (TGA). A DuPont 951 TGA unit was used with a 1090 analyzer. About 25 mg of the sample was reduced in flowing dihydrogen while the temperature was programmed at 10 K min^{-1}. The TGA showed about 4–5 wt% oxygen present as Fe_2O_3.

A dinitrogen BET absorption isotherm was obtained on 954 after the reduction described above. A standard constant-volume incremental-pressure BET was used. The procedure and apparatus has been described elsewhere (*5*). The surface area of the reduced sample was found to be 9.6 m^2 g^{-1} as referred to weight unreduced sample. This is within 10% of the value (8.8 m^2 g^{-1}) reported by Solbakken *et al.* (*4*). It corresponds to an average particle size of 63 nm calculated on the basis of an average value of 9.2 m^2 g^{-1}, a density of metallic iron of 7.87 g cm^{-3} and assuming monodisperse spherical particles.

RESULTS

Mössbauer Effect Spectroscopy

The MES data are shown in Figs. 5 and 6 for the velocity ranges ±10 and ±3 mm s^{-1}, respectively. The spectrum for the unreduced sample (shown in Figs. 5b and 6b) was resolved into two components.

First, there was a magnetite spectrum consisting of 11 peaks (two superimposed

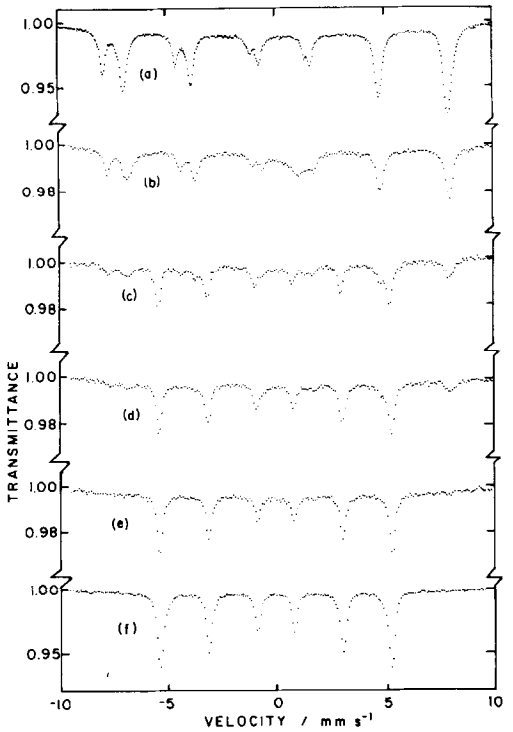

FIG. 5. Mössbauer spectra for 10.2 wt% alumina in magnetite as a function of reduction time at 698 K (±10 mm s^{-1}): (a) pure magnetite (18), (b) unreduced sample, (c) reduced 0.25 h, (d) reduced 0.50 h, (e) reduced 1.50 h, (f) iron foil.

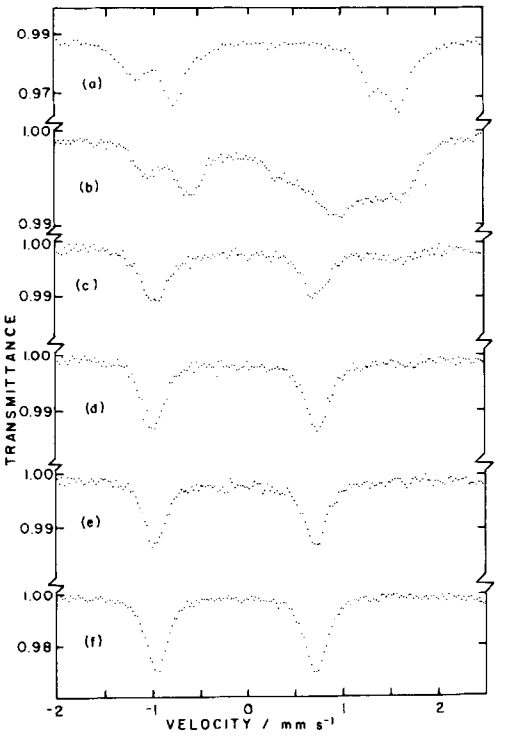

FIG. 6. Mössbauer spectra for 10.2 wt% alumina in magnetite as a function of reduction time at 698 K (±3 mm s^{-1}): (a) pure magnetite (18), (b) unreduced sample, (c) reduced 0.5 h, (d) reduced 1.5 h, (e) reduced 31.5 h, (f) iron foil.

hyperfine spectra). The magnetic fields, defined as

$$H_A = (v_6 - v_1)_A \text{ mm s}^{-1} \times 3.109 \text{ T} \quad \text{(tetrahedral)},$$

and

$$H_B = (v_6 - v_1)_B \text{ mm s}^{-1} \times 3.109 \text{ T} \quad \text{(octahedral)},$$

were $H_A = 48.98T$, $H_B = 45.89T$. The isomer shifts were $\delta_A = 0.163$ mm s^{-1} and $\delta_B = 0.540$ mm s^{-1}. Tables 1 and 2 contain the parameters for the "A" and "B" hyperfine spectra, respectively. A spectrum for pure magnetite (*18*) is also shown in Figs. 5 and 6. Second, a doublet was detected. If it is a quadrupole doublet, the quadrupole splitting and isomer shift are respectively 0.550 and 0.68 mm s^{-1}. This spectral feature can be attributed to wustite (FeO). The area of this feature accounts for 12.8% of the total spectral area. Table 3 lists the spectral parameters for this phase. No background component was detected.

After 0.25 h of reduction, the wustite doublet disappeared, a metallic iron spec-

TABLE 1

Magnetite A (Tetrahedral Sites): Measured Mössbauer Spectral Parameters

	H (T)	ε (mm s^{-1})	δ (mm s^{-1})	Γ_1 (mm s^{-1})	A_T (mm s^{-1})
Magnetite	497	0.010	0.205	0.332	0.064
Unreduced	490	−0.033	0.163	0.302	0.023
0.25-h reduction	487	−0.043	0.168	0.348	0.010
0.5-h reduction	486	−0.005	0.140	0.331	0.005

Note. Γ_1 is the width of the lowest velocity peak.

TABLE 2

Magnetite B (Octahedral Sites): Measured Mössbauer Spectral Parameters

	H (T)	ε (mm s^{-1})	δ (mm s^{-1})	Γ_1 (mm s^{-1})	A_T (mm s^{-1})
Magnetite	462	0.013	0.558	0.409	0.122
Unreduced	459	0.010	0.540	0.572	0.038
0.25-h reduction	460	0.015	0.540	0.628	0.022
0.5-h reduction	459	0.045	0.520	0.699	0.011

Note. Γ_1 is the width of the lowest velocity peak.

trum appeared and the magnetite spectrum diminished (Fig. 5). Through 1.5 h of reduction, the metallic iron spectrum continued to grow in, and the magnetite component disappeared completely. All succeeding spectra contained only the hyperfine spectrum of metallic iron. As can be seen from Table 4, their is no significant variation in the magnetic field and isomer shift of the metallic iron component as reduction proceeds and, in fact, are the same as for an iron foil. No paramagnetic component was detected in the background. The backgrounds obtained from the computer fit for several of the steps in the reduction are shown in Fig. 7 with the very similar backgrounds of Topsøe *et al.* (*14*). The same instrument and computer programs were used in this study and that of Topsøe *et al.*, although the data are not directly comparable since the samples were of different origin. Yet, it can be seen from Fig. 7 that the difference in curves (c) and (d), which indicates the Fe^{2+} detected by Topsøe *et al.* is

TABLE 3

Wustite: Measured Mössbauer Spectral Parameters

	Peak 1	Peak 2	Total
Position (mm s^{-1})	0.40	0.95	—
Width (mm s^{-1})	0.683	0.630	—
Area (mm s^{-1})	0.0026	0.0064	0.0090

Note. Isomer shift = 0.675 mm s^{-1}, quadrupole splitting = 0.55 mm s^{-1}.

TABLE 4

Metallic Iron Measured Mössbauer Spectral Parameters

	H (T)	ε (mm s^{-1})	δ (mm s^{-1})	Γ_1 (mm s^{-1})	A_T (mm s^{-1})
Iron foil	330	0.005	−0.118	0.338	0.137
0.25-h Reduction	331	−0.003	−0.113	0.310	0.037
0.5-h Reduction	331	0.000	−0.115	0.307	0.047
1.5-h Reduction	331	0.002	−0.116	0.295	0.053
4.5-h Reduction	330	0.000	−0.112	0.300	0.061
7.5-h Reduction	331	0.004	−0.113	0.320	0.055
10.5-h Reduction	331	0.004	−0.116	0.320	0.053
13.5-h Reduction	331	0.001	−0.115	0.311	0.053
16.5-h Reduction	331	0.001	−0.116	0.302	0.052
19.5-h Reduction	333	0.001	−0.118	0.301	0.051
25.5-h Reduction	333	0.006	−0.119	0.313	0.050
31.5-h Reduction	333	−0.001	−0.115	0.308	0.054

Note. Γ_1 is the width of the lowest velocity peak.

about the same as the spread of the curves (e)–(j). No trends were detected for the background position (position of maximum dip) nor for the background dip as a function of reduction time. Tables 1–4 contain the pertinent spectral parameters calculated for all the steps of reduction and for the reference materials for these phases, respectively: tetrahedral iron in magnetite, octahedral iron in magnetite, wustite, and metallic iron.

X-Ray Diffraction

The 110 and 220 reflections of metallic iron are shown in Fig. 8 for the iron calibration standard and the reduced, passivated iron–alumina sample. The length of the unit cube, a_0, for iron metal was within 0.1 pm of the reported value (*9*) for both samples. The corrected widths for the iron–alumina sample were 0.190 and 0.238 pm^{-1} for the 110 and 220 reflections, respectively. The paracrystallinity in the 110 direction is 0.57

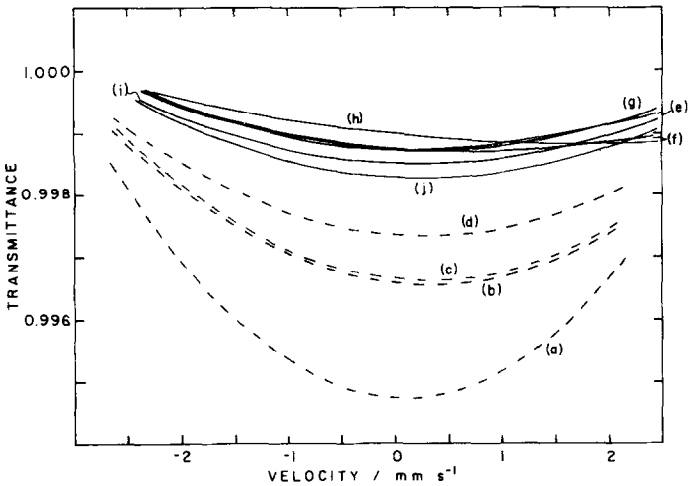

FIG. 7. Calculated backgrounds for various Mössbauer spectra taken in the velocity range of ±3 mm s^{-1}. 2.2 wt% alumina in magnetite (14): (a) passivated sample of Topsøe *et al.* (*14*), (b) reduced in H_2 at 573 K for 0.5 h (14), (c) reduced in H_2 at 688 K for 0.5 h (14), (d) reduced in H_2 at 698 K for 23 h (14). 10.2 wt% alumina in magnetite (reductions at 698 K; cumulative time): (e) reduced 0.5 h, (f) reduced 1.5 h, (g) reduced 4.5 h, (h) reduced 7.5 h, (i) reduced 16.5 h, (j) reduced 31.5 h.

± 0.07%. The crystal size in the 110 direction is 57 ± 3 nm. According to the Scherrer equation (*19*), the calculated crystal size was 49.4 and 39.4 nm for the 110 and 220 reflections, respectively. Assuming that the passivated sample consists of an inner core of iron metal and an outer layer of hematite, these values can be corrected using the densities of iron and hematite as 7.87 and 5.26 g cm^{-3}, respectively. The three crystal sizes above are corrected to 61, 53, and 43 nm, respectively.

DISCUSSION

Mössbauer Effect Spectroscopy

In the unreduced state it should be made clear that the doublet belongs to a wustite

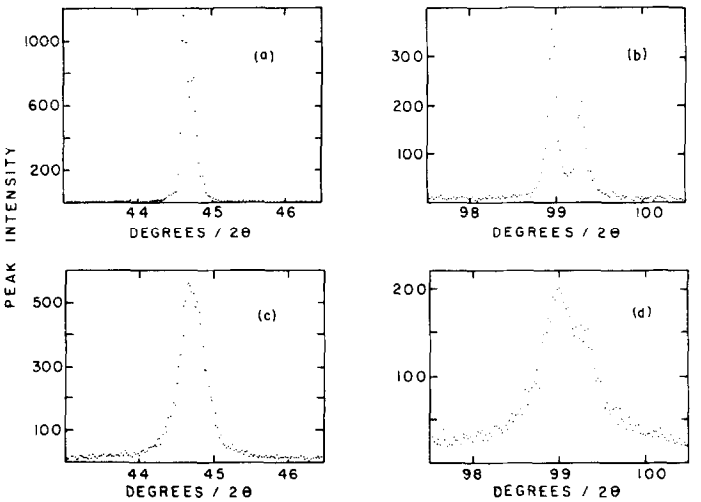

FIG. 8. XRD data. Peak intensity vs angle between source and sample: (a) 110 reflection for the iron standard, (b) 220 reflection for the iron standard, (c) 110 reflection for the iron–alumina sample, (d) 220 reflection for the iron–alumina sample.

phase. Although the wustite phase spectral component does not match exactly (±0.1 mm s^{-1}) that reported in the literature (*20*), the Mössbauer effect for wustite is complex and dependent upon the stoichiometry of the Fe_xO (x is ca. 0.92–0.95) (*20*). The wustite doublet is not similar to any of the forms of hercynite examined in other studies (*21–23*); and wustite has been identified in Mössbauer spectra for industrial ammonia synthesis catalysts (*24*).

The unreduced sample also has lower magnetic fields (49.0, 45.9 T) for the tetrahedral and octahedral sites than that of pure magnetite. The magnetic fields (H_A, H_B) reported for pure magnetite (49.7, 46.2 T) were obtained from a fit of data obtained from a previous study (*18, 25*). Other values reported for H_A and H_B are respectively 49.2, 46.1 T (*18*) and 49.3, 46.5 T (*26*). Also, the first peak of the octahedral (b) spectra is about 40% broader than that of pure magnetite (*18, 25*). Using MES, Garbassi *et al.* (*26*) measured the absorption peak linewidths and magnetic fields for magnetite with varying amounts of alumina. In comparison with data from Garbassi *et al.*, it appears that only 10% of the total alumina has gone into solid solution with the magnetite in our sample. These data do not exclude the possibility mentioned by Ludwiczek *et al.* (*9*) that all of the alumina is in solid solution with the magnetite for samples prepared in a different manner. In our unreduced sample there is an association of some of the Al_2O_3 with the Fe_3O_4. The rest of alumina, therefore, is in a separate phase from the magnetite. This was confirmed by scanning electron microscopy, which detected alumina particles as large as 50 μm in the unreduced sample.

The wustite phase was reduced in 0.25 h. This reduction is faster than that of magnetite as reported in studies on industrial catalysts (*24*). Reduction of the magnetite component is faster (1.5 h) than that reported by Ludwiczek *et al.*, 144 h (*9*). However, the 1.5 h is comparable to the work on multipromoted samples by Baranski *et al.* (*27*).

The arguments of Topsøe *et al.* (*14*) were used to reach the following conclusions. First, the change in the iron magnetic field for dilute Fe–Al alloys (*28*) is about 0.2 T per 1 mol% of aluminum. Considering the variation in the magnetic field of the metallic iron phase (0.3 T), the concentration of aluminum inside the iron crystals present as randomly distributed $FeAl_2O_4$ molecules is less than 0.75 mol%. Thus, at most, 10% of the total alumina exists inside the iron crystals in this form. Second, the area between the calculated background curves (g) and (j) of Fig. 7 is equivalent to the area between curves (c) and (d) which were calculated from the spectra for the sample studied by Topsøe *et al.* (*14*). These areas correspond to 1.5% of the total iron area indicating that 1.5% of the iron is Fe^{2+}. Therefore, the deviation in the background curves indicates that ca. 15% of the total alumina can exist as $FeAl_2O_4$. The results of the magnetic field measurements and the background measurements are in agreement with the results measured for the unreduced state: 10% of the total alumina is inside the iron.

X-Ray Diffraction

A comparison of iron crystal size (61 nm) obtained from XRD and iron particle size (63 nm) obtained from specific area indicates that the iron particles are single crystals. However, with the assumption of single crystal spherical particles, crystals with a diameter of 25 nm, as measured by Hosemann *et al.* (*6*) and other workers (*1*), would have a surface area of 30 m^2 g^{-1}. Since this latter value is much larger than has ever been reported for any promoted, unsupported iron material, these XRD crystal size measurements indicate polycrystalline particles of iron.

The crystal sizes obtained in this work by the Scherrer equation (53 and 43 nm) are slightly smaller than that measured by the technique of Fischer *et al.* (*7*). Since the calculated crystal size decreased from the

110 to the 220 reflection, the linewidths had broadened more than would be expected by crystal size alone. This supports the of paracrystallinity for our material. The detection of paracrystallinity suggests the possibility that some of the alumina exists inside the iron crystals as hercynite. However, the paracrystallinity for the 110 direction measured for our iron–alumina sample was lower than that measured by Ludwiczek *et al.* (*9*) on a reduced sample containing 1.0 wt% Al_2O_3 in Fe_3O_4. They measured 0.81% paracrystallinity as opposed to 0.57% measured for the 10.2 wt% Al_2O_3 sample of this study. Since the paracrystallinity of our sample is smaller than the paracrystallinity of their sample, the amount of alumina inside the iron crystals of our sample must be smaller than that of theirs: <1 wt%. This estimated amount is confirmed by the MES results.

Location of the Alumina

The results of both the MES and XRD experiments indicate that not more than 10% of the total alumina can be inside the reduced iron crystals. This means that the amount of alumina in iron is ca. 1 wt%. This small amount of alumina inside the iron crystals has been confirmed by X-ray absorption spectroscopy and the associated extended X-ray absorption fine structure. These results are, however, preliminary (*29*). Hosemann and co-workers have suggested that the form of the aluminum oxide inside the iron particles is $FeAl_2O_4$ as shown in Fig. 3. Another possibility might be Al_2O_3 (Fig. 9). The volume of the three oxygen ions is *about* the same as that of five metallic iron atoms (*6*). The volume of the aluminum ions is neglected. But the first eventuality seems preferable since the lattice spacing of iron in the reduced samples is identical to that of pure iron.

The unreduced state as described by Hosemann and co-workers should have only one MES component. Also, the reduced sample should have a smaller magnetic field than iron metal with a paramagnetic component (*14*), plus at least 1% paracrystallinity. These results were not observed for our sample. According to the model of Pernicone *et al.* (*8, 10*), an iron–alumina material would have a paramagnetic component after reduction. Since that was not the case here, the present sample must not have had these clusters. The investigation done by Topsøe *et al.* (*14*) showed a reducible background component which was not detected here. The data obtained for our sample does not support their model of hercynite inclusions that can be reduced to alumina inclusions. Although the temperature–time profile of their reduction was different than the one used here, their sample had already been reduced and passivated. The difference in sample preparations between our sample and that of the other workers can perhaps account for the different experimental observations.

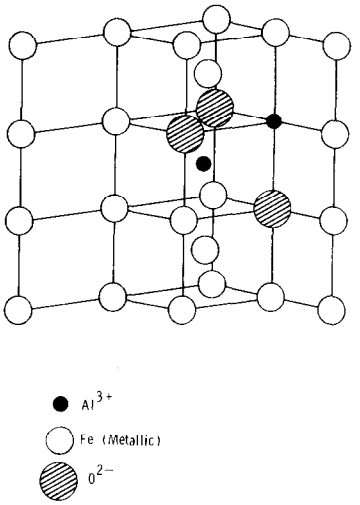

FIG. 9. Alumina in the α-iron lattice.

Surface area measurements that were done on our reduced sample indicated that the alumina existed as 50% of a monolayer on the surface of the iron particles (*2–5*). This accounts for ca. 5% of the total alumina. With the amount of alumina determined to be inside the iron particles in this work, only 15% of the alumina has been accounted for. This means that 85% of the alumina exists either at the grain bound-

aries of the iron crystals and/or in a separate external phase. The former is a more reasonable location since that alumina would not be detected by XRD or surface concentration measurements. However, there is no direct evidence for alumina to be at grain boundaries. In summary, the Al_2O_3 appears to be located in the reduced sample as follows 10% inside iron particles as Al_2O_3 or $FeAl_2O_4$, 5% on the surface of the iron particles as Al_2O_3, and 85% at grain boundaries or in a separate phase as Al_2O_3.

The Mode of Textural Promotion

According to the theory of Schultz (*13*), this amount of alumina or hercynite in iron (1 wt%) cannot promote the iron by surface relaxation of internal stress. The defect concentration is below the critical values of Schultz's plot.

The data for this sample (954) support both of the correlations mentioned above concerning crystal size and paracrystallinity. The data for this sample are at the edge of the correlation of Fischer *et al.* (*7*), i.e., $\alpha^* = 0.10$. Also, they fall on the line of Fig. 4. Further, the average reduced iron *particle* size is the same as the average reduced iron *crystal* size for this sample. This suggests that paracrystallinity is related to particle size and causes textural promotion. However, this is the only sample for which this is demonstrated. Single crystal particles were also claimed by Fischer *et al.* (*7*) for their model catalyst, but the surface area was not reported.

Another mode of textural promotion of iron by alumina in this sample is a patchy "skin" effect: the alumina partially covers the surface of the reduced iron particles which prevents the iron atoms on adjacent particles from coalescing.

Further work is necessary to decide which mode of textural promotion dominates. But if paracrystallinity can produce a smaller particle size, as would be expected with single crystal particles, an improved catalyst may be possible with small additions of alumina. Commercial ammonia synthesis catalysts have a total surface area of ca. 10–15 $m^2\ g^{-1}$, but less than 10% of this area is active iron. If a catalyst could be made without surface promoters but with the same total surface area as a conventional catalyst as a result of stabilization by paracrystallinity due to dissolved alumina or hercynite, then the catalyst would have a higher specific surface area of active iron than currently available. That this could be achieved is only speculation.

CONCLUSIONS

Approximately 10% of the total alumina is dissolved in the Fe_3O_4 in the unreduced sample. The wustite and the magnetite phases reduce to metallic iron. The distribution of the Al_2O_3 in the reduced sample is 10% inside the iron particles, 5% on the surface, and 85% at grain boundaries or in another phase.

Both published correlations between paracrystallinity and crystal size are supported by the data presented above. For our reduced sample the average iron *particle* size is the same as the average iron *crystal* size. Since our work provides the only data relating paracrystallinity and surface area, further work is necessary to establish the importance of paracrystallinity in textural promotion.

REFERENCES

1. Nielsen, A., "An Investigation on Promoted Iron Catalysts for the Synthesis of Ammonia," 2nd ed., Jul. Gjellerups, Copenhagen, 1956; Nielsen, A. *in* "Advances in Catalysis" (W. G. Frankenburg *et al.* eds.), Vol. 5, p. 10. Academic Press, New York, 1953.
2. Emmett, P. H., and Brunauer, S., *J. Amer. Chem. Soc.* **59,** 310 (1937).
3. Emmett, P. H., and Brunauer, S., *J. Amer. Chem. Soc.* **59,** 1553 (1937).
4. Solbakken, V., Solbakken, A., and Emmett, P. H., *J. Catal.* **15,** 90 (1969).
5. Silverman, D. C., and Boudart, M., *J. Catal.* **77,** 208 (1982).
6. Hosemann, R., Preisinger, A., and Vogel, W., *Ber. Bunsenges. Phys. Chem.* **70,** 796 (1966).
7. Fischer, A., Hosemann, R., Vogel, W., Kouteck, J., and Ralek, M., *Int. Congr. Catal. Tokyo prepr. A22* (1980).

8. Fagherazzi, G., Galante, F., Garbassi, F., and Pernicone, N., *J. Catal.* **26,** 344 (1972).
9. Ludwiczek, H., Preisinger, A., Fischer, A., Hosemann, R., Schonfeld, A., and Vogel, W., *J. Catal.* **51,** 326 (1978).
10. Pernicone, N., Fagherazzi, G., Galante, F., Garbassi, F., Lazzerin, F., and Mattera, A., *in* "Proceedings, 5th International Congress on Catalysis, Amsterdam, 1972" (J. W. Hightower, Ed.), p. 1241. North-Holland, Amsterdam, 1972.
11. Buhl, R., and Preisinger, A., *Surf. Sci.* **47,** 344 (1975).
12. Hosemann, R., Fischer, A., and Ralek, M., *Phys. Bull.* **36,** 334 (1980).
13. Schultz, J. M., *J. Catal.* **27,** 64 (1972).
14. Topsøe, H., Dumesic, J. A., and Boudart, M., *J. Catal.* **28,** 477 (1973).
15. Wyckoff, R. W. G., and Crittenden, E., *J. Amer. Chem. Soc.* **47,** 2866 (1925).
16. Brunauer, S., and Emmett, P. H., *J. Amer. Chem. Soc.* **62,** 1732 (1940).
17. Maxwell, L. R., Smart, J. S., and Brunauer, S., *J. Chem. Phys.* **19,** 303 (1951).
18. Topsøe, H., Ph.D. thesis, Stanford University, Stanford, Calif., 1973.
19. Warren, B. E., "X-Ray Diffraction," Addison–Wesley, Menlo Park, Calif., 1969.
20. Checherskaya, L. F., Romanov, V. P., and Tatsienko, P. A., *Phys. Status Solidi A* **19,** K177 (1973).
21. Yagnik, C. M., and Mathur, H. B., *J. Phys.* **1,** C2–469 (1968).
22. Rossitner, M. J., *J. Phys. Chem. Solids* **26,** 775 (1965).
23. Ono, K., Ito, A., and Syono, Y., *Phys. Lett.* **19,** 620 (1965).
24. Clausen, B. S., Mørup, S., Topsøe, H., Candia, R., Jensen, E. J., Baranski, A., and Pattek, A., *J. Phys.* **37,** C6–245 (1976).
25. Magnetite Mössbauer data from Ref. (*18*) were analyzed by the procedures used in this study to facilitate comparisons between pure magnetite and the sample of this work.
26. Garbassi, F., Fagherazzi, G., and Calcaterra, M., *J. Catal.* **26,** 338 (1972).
27. Baranski, A., Lagan, M., Pattek, A., Reizer, A., Christiansen, L. J., and Topsøe, H., *in* "Proceedings, Second International Symposium on the Scientific Bases for the Preparation of Heterogeneous Catalysts, Louvain-La-Neuve, Belgium, Sept. 1978," p. 353. Elsevier, Amsterdam, 1979.
28. Johnson, C. E., Ridout, M. S., and Cranshaw, T. E., *Proc. Phys. Soc. London* **81,** 1079 (1963).
29. Borghard, W. S., Ph.D. thesis, Stanford University, Stanford, Calif., 1982.